IEEE Access
Multidisciplinary ⋮ Rapid Review ⋮ Open Access Journal

Received 25 January 2024, accepted 22 March 2024, date of publication 28 March 2024, date of current version 15 April 2024.

Digital Object Identifier 10.1109/ACCESS.2024.3382538

RESEARCH ARTICLE

Delay Compensation and Outlier Removal in Command Signal for Teleoperated Vehicle Using Asynchronous Filter

EUGENE KIM, HYUNROK CHA, TERESSA TALLURI, CHANYEONG JEONG, HYEONWOO KIM, SEUNGHA YOON, AND MYEONGHWAN HWANG

Korea Institute of Industrial Technology, Gwangju 61012, Republic of Korea

Corresponding author: Myeonghwan Hwang (han9215@kitech.re.kr)

This work was supported by Korea Institute of Industrial Technology as "Development of Core Technologies for a Working Partner Robot in the Manufacturing Field" under Grant KITECH EO-23-0009.

ABSTRACT We propose an evaluation metric for communication status that classifies the communication delay as passive, additive, and temporary communication delay and an asynchronous delay compensation Kalman filter with an outlier rejection strategy. Experimental and simulation results demonstrate the kalman filter's ability to handle both additive and temporal communication delays, contributing to improved safety integrity in line with ISO 26262 requirements. The result shows that the proposed filter can resist not only additive communication delays but also can resist temporal communications delays.

INDEX TERMS Communication sensor delay compensation, Kalman filter, sensor signal delay, safety-integrity level, teleoperated vehicle.

I. INTRODUCTION

With the rapid advancement of autonomous driving and connected communication technologies, several Original Equipment Manufacturers (OEMs) and research institutes are leading towards the commercialization of autonomous vehicles [1], [2], [3]. Typically, the degree of autonomous driving is classified in stages from L0 (No driving automation) to L5 (Full driving automation), and the Dynamic Driving Tasks (DDT) function is required in the L3-5 stage [4]. Humans perform Object and Event Detection and Response (OEDR) for vehicles below L3 as the boundary, but for autonomous vehicles above L3, the vehicle system can perform this role. In particular, in the case of autonomous vehicles of SAE L4 or higher, according to the international standards of SAE J3016 and ISO 22736, the autonomous driving system detects an emergency state to execute DDT Fallback function [4], [5]. However, it is not feasible to provide a response guide for them one by one in an edge case such as a situation where vehicles and pedestrians are congested.

The associate editor coordinating the review of this manuscript and approving it for publication was Zheng Chen.

According to the disengagement report released by the California State Transportation Agency (CalSTA), there are often situations in which accidents can occur when the driver does not intervene during test driving of autonomous vehicles [6]. Among them, recognition failure and software problems mostly accounted and the autonomous driving function was canceled by a human test driver, or in some cases, intervention in the autonomous driving vehicle system was carried out. In addition, the disengagement of the autonomous driving function has been reported regardless of road, intersection, and highway, and in some cases, it is expected that an accident would have occurred without the intervention of a human test driver. However, it is necessary to return to the minimum risk state as soon as possible by the autonomous vehicle in a situation where a human driver does not reside with L4 or higher [4]. Therefore, the disengagement of autonomous driving can lead to a cause of hindering vehicle traffic, which is also a great issue in terms of the agility of the transportation system.

A. TELEOPERATION AND COMMUNICATION DELAY

As a remedy for the disengagement of autonomous driving, the concept of teleoperation can be utilized. However, the

teleoperation of an actual vehicle has been implemented only in limited situations due to the diversity of application cases of autonomous vehicles and the performance of computational and communication [7]. Recently, with the development of computational performance and improvement of the cellular network environment, teleoperation is being studied in depth, and research on the human-machine interface is actively in progress [8]. Zheng.et al. made a proposal for the establishment of a control center to control vehicle emergency situations, remote control of the vehicle, and real-time interface [7], [9]. Basso. et al. presented a method of teleoperation of a military jeep using a single camera in the off-road environment [10]. In fact, already some commercialized services were introduced to conduct teleoperation for industrial forklift trucks [11]. Further, a celebrated usage of teleoperation schemes can be widely found in the robots field for their control systems targeting teleoperation [12], [13]. Especially, due to the sensory feedback and wireless technology improvements, teleoperation span from rehabilitation, surgery, aerospace field, and to unmanned air crafts [14], [15], [16].

On the other hand, numerous efforts have been taken to classify communication delays and reduce their effects. Yao. et al. made a communication delay analysis based on the wireless IEEE 802.11p protocols in the highway environment and shown exponential distribution is the best approximation to explain the access delay profiles [17]. In addition, Kim. et al. proposed a delay-tolerant intersection management protocol and classified the situations based on the preliminarily determined scenarios to prevent safety issues [18], [19]. However, few studies were conducted on end-to-end communication analysis and on the tolerant system and most of them were tested by applying simulation [20].

One of the sophisticated methods to estimate a state stochastically is using the kalman filtering approach [21], [22], [23]. When applying the Kalman filter to outlier coexisting environments, it is effective to implement robust strategies such as compensation-based and rejection-based noise managing processes [24], [25], [26], [27], [28], [29]. By far of the authors' knowledge, despite numerous robust Kalman filter techniques being introduced to remove outliers, few discussions were made at the communication level for remote control usage. In this study, we propose an asynchronous delay compensation Kalman filter for compensation of the communication delay and rejection of outlier in the signal that severely differs from the expected communication delay.

B. CONTRIBUTIONS

The contributions of this study consist of two main ideas.

1) The proposed filter can remove additive and temporary communication delay outliers
2) Introduction of a stochastic heavy-tailed Gaussian delay model that can generate realistic communication delay outliers.

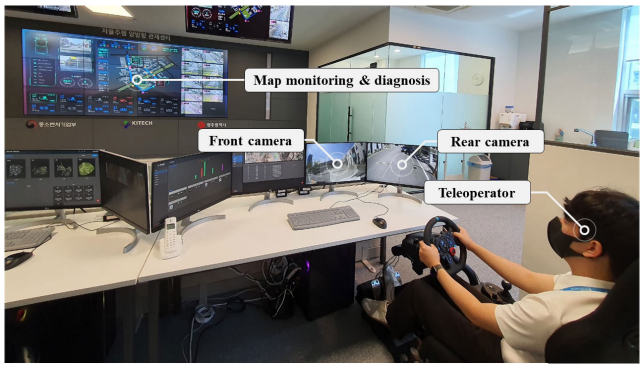

FIGURE 1. Example of teleoperation service using remote control device and visualization apparatus. Teleoperation is challenging in terms of delay management and limitations of methods for transmitting environmental information to the human operator.

In this study, an asynchronous delay compensation Kalman filter is proposed as a potential solution for compensating for communication delays and rejecting outliers.

By using the proposed delay model, the occurrence probability of actual communication delay outliers can be controlled, which can be utilized for the performance evaluation of delay compensation filters such as the proposed filter.

II. METHODOLOGY

Fig. 1 shows an example of a teleoperation service provided by a control center. The teleoperation of the vehicle is different from the traditional local control method in that the teleoperated target and the vehicle controlling unit are physically separated. In particular, compared to conventional local communication-based control methods, the teleoperation command implies distinctive uncertainty due to the communication delay. Therefore, in this section, we propose a concept of a novel filter based on the evaluation of the system including the uncertainty of command signal due to telecommunication.

A. UNSCENTED KALMAN FILTER

An asynchronous delay compensation kalman filter with a pseudo observation vector has been briefly explained in this section. In advance, the symbol $\wedge$ denotes estimated values. Also, $(-)$ and $(+)$ represent priori and posterior estimations of the state of the model, respectively.

First, we consider the discrete-time nonlinear stochastic state-space model when using an unscented Kalman filter (UKF) [30], [31]. The typical system of the nonlinear dynamic model can be expressed as:

$$\mathbf{x}_k = f(\mathbf{x}_{k-1}, dt) + \mathbf{w}_k, \tag{1}$$

where $\mathbf{x}_k$ is the n-dimensional state space vector at discrete-time k, f denotes the transition function, $\mathbf{w}_k$ represents the process noise which follows the Gaussian distribution, and dt is an interval of time between the samples.

Next, the state estimation process can be conducted after receiving the measurements as follows:

$$\mathbf{z}_k = h(\mathbf{x}_k) + \mathbf{v}_k, \tag{2}$$

where $\mathbf{z}_k$ represents the m-dimensional observation vector at discrete-time k, h denotes the observation function, and $\mathbf{v}_k$ means a measurement noise also following the Gaussian distribution.

Let χ is a set of $2n+1$ sigma points that deviates from the original mean and covariance of the state space vector:

$$\begin{aligned}
\chi_{k-1}^{(0)} &= \mathbf{x}_{k-1} \\
\chi_{k-1}^{(i)} &= \mathbf{x}_{k-1} + \sqrt{n+\lambda}[\sqrt{\mathbf{P}_{k-1}}]_i \\
\chi_{k-1}^{(i+n)} &= \mathbf{x}_{k-1} - \sqrt{n+\lambda}[\sqrt{\mathbf{P}_{k-1}}]_i (i = 1, \ldots, n),
\end{aligned} \tag{3}$$

where, $\mathbf{m}$ is the mean value sets of the sigma points, and $\mathbf{P}$ is the covariance matrix for each state space component respectively. Also, λ represents a scaling parameter determined as $\lambda = \alpha^2(n+\kappa) - n$, where α and κ is the parameter that determines the spread of the sigma points.

Then propagation process can be carried out through the transition function using sigma points:

$$\hat{\chi}_k^{(i)} = f(\chi_{k-1,dt}^{(i)}) \quad \text{for } i = 0, 1, \ldots, 2n, \tag{4}$$

where, $\hat{\chi}$ is predicted set of sigma points. Therefore, the weighted mean and covariance matrices for the set of the sigma points can be written as:

$$\mathbf{x}_k^- = \sum_{i=0}^{2n} W_i^{(m)} \hat{\chi}_k^{(i)} \tag{5}$$

$$\mathbf{P}_k^- = \sum_{i=0}^{2n} W_i^{(c)} (\hat{\chi}_k^{(i)} - \mathbf{m}_k^-)(\hat{\chi}_k^{(i)} - \mathbf{m}_k^-)^{\mathrm{T}} + \mathbf{Q}_{k-1} \tag{6}$$

where $\mathbf{m}_k^-$ is the priori weighted mean vector, $\mathbf{P}_k^-$ is the priori covariance matrix predicted from the sets of the sigma points at discrete-time k respectively. In addition, weights $W_i^{(m)}$ and $W_i^{(c)}$ are given as follows:

$$W_0^{(m)} = \lambda/(n+\lambda) \tag{7}$$

$$W_0^{(c)} = \lambda/(n+\lambda) + (1 + \alpha^2 + \beta) \tag{8}$$

$$W_i^{(m)} = 1/2(n+\lambda), \text{for } i = 1, 2, \ldots, n \tag{9}$$

$$W_i^{(c)} = 1/2(n+\lambda), \text{for } i = 1, 2, \ldots, n, \tag{10}$$

where β is the parameter utilized for the prior information of the distribution of state space vector $\boldsymbol{x}$. Hence, the remapped priori sigma points χ^- can be written using the mean and covariance matrices:

$$\begin{aligned}
\chi_k^{-(0)} &= \mathbf{x}_k^- \\
\chi_k^{-(i)} &= \mathbf{x}_k^- + \sqrt{n+\lambda}[\sqrt{\mathbf{P}_k^-}]_i \\
\chi_k^{-(i+n)} &= \mathbf{x}_k^- - \sqrt{n+\lambda}[\sqrt{\mathbf{P}_k^-}]_i (i = 1, \ldots, n).
\end{aligned} \tag{11}$$

Algorithm 1 Unscented Kalman filter

Input : $\mathbf{x}_{k-1}^+, \mathbf{z}_{k-1}^+, \mathbf{P}_{k-1}^+$
Output $\mathbf{x}_k^+, \mathbf{P}_k^+$
:
Generate 2n+1 sigma points: $\chi_{k-1}^{(i)}$;
Propagation process:
$\hat{\chi}_k^{(i)} = f(\chi_{k-1}^{(i)}, dt)$ for $i = 0, 1, \ldots, 2n,$;
Prediction of priori mean:
$\mathbf{x}_k^- = \sum_{i=0}^{2n} W_i^{(m)} \hat{\chi}_k^{(i)}$;
Prediction of priori covariance:
$\mathbf{P}_k^- = \sum_{i=0}^{2n} W_i^{(c)} (\hat{\chi}_k^{(i)} - \mathbf{m}_k^-)(\hat{\chi}_k^{(i)} - \mathbf{m}_k^-)^{\mathrm{T}} + \mathbf{Q}_{k-1}$;
Measurement model during propagation:
$\hat{\zeta}_k^{(i)} = h(\chi_k^{-(i)})$ for $i = 0, 1, \ldots, 2n$;
Compute representative of propagated sigma points:
$\mu_{\boldsymbol{k}} = \sum_{i=0}^{2n} W_i^{(m)} \hat{\zeta}_k^{(i)}$;
Calculate kalman gain:
$\boldsymbol{K}_k = \boldsymbol{C}_k \boldsymbol{S}_k^{-1}$;
$\boldsymbol{S}_k = \sum_{i=0}^{2n} W_i^{(c)} (\hat{\zeta}_k^{(i)} - \mu_k)(\hat{\zeta}_k^{(i)} - \mu_k)^{\mathrm{T}} + \boldsymbol{R}_k$;
$\boldsymbol{C}_k = \sum_{i=0}^{2n} W_i^{(c)} (\chi_k^{-(i)} - \mathbf{x}_k^-)(\hat{\zeta}_k^{(i)} - \mu_k)^{\mathrm{T}}$;
Estimation of posterirori mean:
$\mathbf{x}_k^+ = \mathbf{x}_k^- + \boldsymbol{K}_k(\tilde{\mathbf{z}}_k - \mu_k)$;
Estimation of posterirori covariance:
$\boldsymbol{P}_k^+ = \boldsymbol{P}_k^- - \boldsymbol{K}_k \boldsymbol{S}_K \boldsymbol{K}_k^{\mathrm{T}}$;
return $\mathbf{x}_k^+, \boldsymbol{P}_k^+$

Therefore, measurement model during propagation of sigma points can be written as follows:

$$\hat{\zeta}_k^{(i)} = h(\chi_k^{-(i)}) \quad \text{for } i = 0, 1, \ldots, 2n \tag{12}$$

where $\hat{\zeta}$ is observable propagated set of sigma points. Then the representative value of the propagated sigma points μ_k can be calculated with:

$$\mu_{\boldsymbol{k}} = \sum_{i=0}^{2n} W_i^{(m)} \hat{\zeta}_k^{(i)}. \tag{13}$$

Further, Kalman gain can be computed with measurement residual covariance $\boldsymbol{R}$ as follows:

$$\boldsymbol{K}_k = \boldsymbol{C}_k \boldsymbol{S}_k^{-1} \tag{14}$$

$$\boldsymbol{S}_k = \sum_{i=0}^{2n} W_i^{(c)} (\hat{\zeta}_k^{(i)} - \mu_k)(\hat{\zeta}_k^{(i)} - \mu_k)^{\mathrm{T}} + \boldsymbol{R}_k \tag{15}$$

$$\boldsymbol{C}_k = \sum_{i=0}^{2n} W_i^{(c)} (\chi_k^{-(i)} - \mathbf{x}_k^-)(\hat{\zeta}_k^{(i)} - \mu_k)^{\mathrm{T}}, \tag{16}$$

where $\boldsymbol{S}_k$ is the error covariance matrix of observational sigma points between the representative value of the predicted observable sigma points, and $\boldsymbol{C}_k$ is the joint covariance matrix between the propagated sigma points residuals and that of the observable sigma points. Finally, the estimated state space

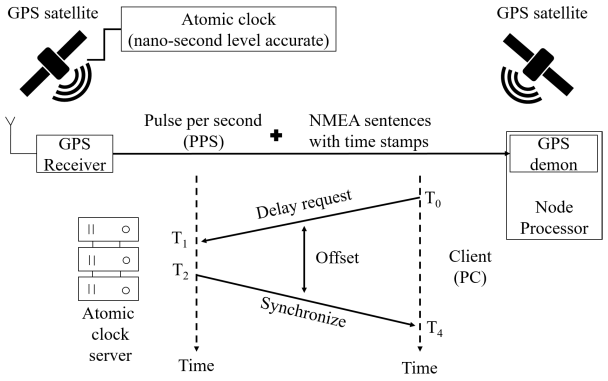

FIGURE 2. Illustration of time synchronization using GPS and pulse per second signal. Theoretical precision of synchronized inner clock of the client PC using network time protocol is nano-second level.

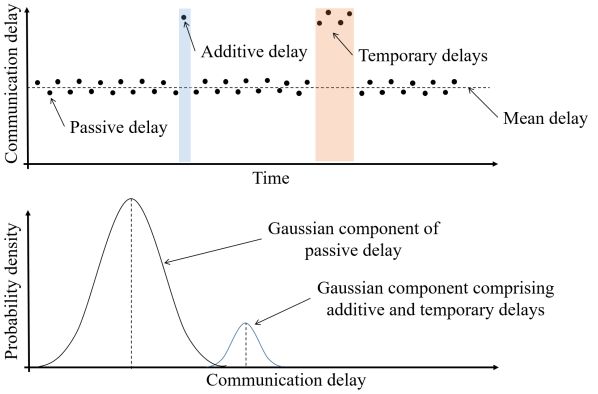

FIGURE 3. Classification of delays depending on the magnitude of the communication delay: Passive delay (PD), Additive delay (AD), Temporary delay (TD). In this study, the Gaussian mixture model was implemented to distinguish the outlier from the passive delays.

vector and covariance matrix can be written as follows:

$$\mathbf{x}_k^+ = \mathbf{x}_k^- + \boldsymbol{K}_k(\tilde{\boldsymbol{z}}_k - \mu_k) \tag{17}$$

$$\boldsymbol{P}_k^+ = \boldsymbol{P}_k^- - \boldsymbol{K}_k \boldsymbol{S}_K \boldsymbol{K}_k^{\mathrm{T}}, \tag{18}$$

where $\tilde{\boldsymbol{z}}_k$ is the actual measured value. The equations and algorithms of the unscented kalman filter is briefly explained and summarized in Algorithm 1.

B. CLASSIFICATION OF COMMUNICATION DELAYS AND OBSERVATION OF COMMUNICATION DELAY

Despite upper efforts of reducing the uncertainties of estimation, the Kalman filter approach can be effective only when the prerequisites hold which measurement noise is Gaussian. In fact, the communication delay is one of the core safety issues when controlling a teleoperated vehicle. However, measuring the communication delay is challenging especially when the vehicle system and the controlling interface are connected wirelessly due to each unit having its own inner clocks. One of the effective delay measurement techniques in a remote network system is utilizing time information in the global positioning system (GPS). As shown in Fig. 2, in order to achieve a precisely synchronized inner clock system, network time protocol (NTP) can be used as an option [32] In this study, the communication delay was measured by comparing each of the synchronized inner clock information from the controlling units using NTP and GPS signals.

Further, as shown in Fig. 3, we classify the communication delay into a passive delay (PD), additive (AD), and temporary delay (TD) which both can be regarded as an outlier. PD refers to the inherent communication delay introduced mainly due to the physical properties of the communication circumstances. Further, AD refers to a communication delay outlier introduced into the communication system that has a single perturbation. Finally, TD refers to communication delay outliers that have multiple perturbations. In this study, we assume that both passive delay and outliers are originating from non-identical Gaussian distribution. In order

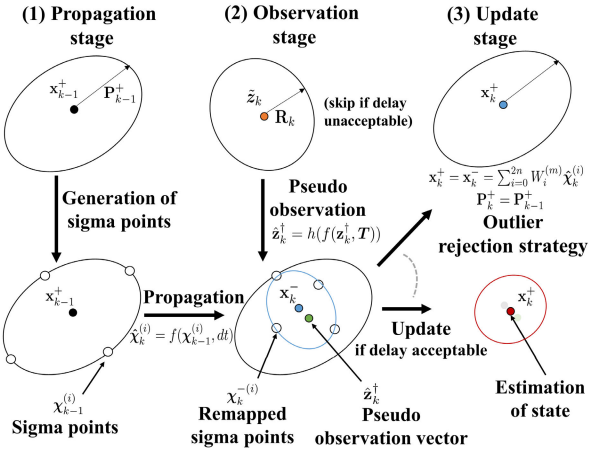

FIGURE 4. Schematic diagram of proposed filter algorithm that rejecting communication delay outliers.

to distinguish the measured delay $\boldsymbol{T}$ for which type of delay is more responsible, the measurement delay is profiled based on the Gaussian mixture distribution:

$$p(\boldsymbol{T}) = \sum_{d}^{D} p(\theta_d) p(\boldsymbol{T}|\theta_d) = \sum_{d=1}^{D} \pi_d \mathcal{N}(\boldsymbol{T}|\mu_d, 6_d), \tag{19}$$

where θ_d is a D-dimensional binary random variable, π_d is the mixing coefficients satisfying $0 \leq \pi_d \leq 1$, μ_d is the mean vector, and 6_d is the covariance matrix of the Gaussian distribution ($\mathcal{N}$). Further, a conditional probability of θ when the $\boldsymbol{T}$ is given can be calculated as:

$$\gamma(\theta_d) \equiv p(\theta_d = 1|\boldsymbol{T}) = \frac{\pi_d \mathcal{N}(\boldsymbol{T}|\mu_d, 6_d)}{\sum_{d=1}^{D} \pi_d \mathcal{N}(\boldsymbol{T}|\mu_d, 6_d)}, \tag{20}$$

where $\gamma(\theta_d)$ corresponds to the responsibility of posterior distribution after observing $\boldsymbol{T}$. In this study, $\gamma(\theta_d)$ was used as an outlier judging criterion for each measured time delays.

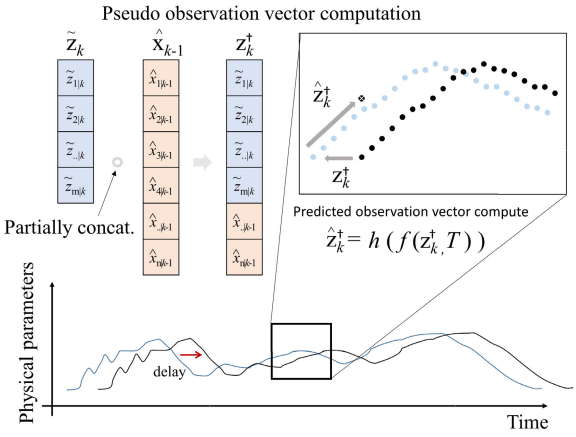

FIGURE 5. Schematic diagram showing the process of computing the predicted observation vector.

C. ASYNCHRONOUS DELAY COMPENSATION KALMAN FILTER

When the communication delay is relatively constant and acceptable, the residuals originating in the delay can be compensated using the transition function. Fig .4 shows the concept of the proposed delay compensation strategy. First, in order to reduce the effect of the passive delays, the observation vector was reorganized to meet the required dimension of the transition model:

$$\mathbf{z}_k^{\dagger} = \left[\tilde{z}_{1|k} \ \ldots \ \tilde{z}_{m|k} \ \hat{x}_{m-n+1|k-1} \ \ldots \ \hat{x}_{n|k-1}\right]^{\mathrm{T}}, \tag{21}$$

where $\mathbf{z}_k^{\dagger}$ is the pseudo observation vector.

As shown in Fig. 5 the predicted observation vector was computed using the transition function:

$$\hat{\mathbf{z}}_k^{\dagger} = h(f(\mathbf{z}_k^{\dagger}, \boldsymbol{T})), \tag{22}$$

where $\hat{\mathbf{z}}_k^{\dagger}$ is the predicted observation vector considering the communication delays. It should be noted that the noise of the measured observation vector is assumed to follow a Gaussian distribution:

$$\mathbf{v}_k \sim \mathcal{N}(0, \mathbf{R}), \tag{23}$$

where $\mathcal{N}$ represents Gaussian distribution. However, by using the pseudo observation process, now the predicted observation vector meets the following:

$$\hat{\mathbf{z}}_k^{\dagger} \sim \mathcal{N}(h(\boldsymbol{x}_k), \mathbf{Q}_k), \tag{24}$$

when the one-way communication delay is measured precisely. Therefore the estimated state space vector when the measured delay is passive can be rewritten as follows:

$$\mathbf{x}_k^{+} = \mathbf{x}_k^{-} + \boldsymbol{K}_k(\hat{\mathbf{z}}_k^{\dagger} - \mu_k). \tag{25}$$

Algorithm 2 Asynchronous Delay Compensation Kalman Filter

Input : $\mathbf{x}_{k-1}^{+}, \mathbf{z}_{k-1}^{+}\ \mathbf{P}_{k-1}^{+}$
Output $\mathbf{x}_k^{+}, \mathbf{P}_k^{+}$
:
Conduct 1-7 of the UKF sequence (Algorithm 1);
Estimation of communication delay:
$\gamma(\theta_d) \equiv p(\theta_d = 1|\boldsymbol{T})$;
Compute pseudo observation vector:
$\mathbf{z}_k^{\dagger} = [\tilde{z}_{1|k} \ldots \tilde{z}_{m|k}\ \hat{x}_{m-n+1|k-1} \ldots \hat{x}_{n|k-1}]^{\mathrm{T}}$;
Predicted pseudo observation vector:
$\hat{\mathbf{z}}_k^{\dagger} = h(f(\mathbf{z}_k^{\dagger}, \boldsymbol{T}))$;
Estimation of state space vector:
if $\gamma(\theta_o) > \gamma(\theta_p)$ *and* $\tau \geq 2$ **then**
  $\mathbf{x}_k^{+} = \mathbf{x}_k^{-} = \sum_{i=0}^{2n} W_i^{(m)} \hat{\chi}_k^{(i)}$
  $\mathbf{P}_k^{+} = \mathbf{P}_{k-1}^{+}$;
else
  $\mathbf{x}_k^{+} = \mathbf{x}_k^{-} + \boldsymbol{K}_k(\hat{\mathbf{z}}_k^{\dagger} - \mu_k)$;
  $\boldsymbol{P}_k^{+} = \boldsymbol{P}_k^{-} - \boldsymbol{K}_k \boldsymbol{S}_K \boldsymbol{K}_k^{\mathrm{T}}$;
end
return $\mathbf{x}_k^{+}, \boldsymbol{P}_k^{+}$

Finally, the error covariance matrix of observational sigma points and the posterior covariance matrix can be written as:

$$\boldsymbol{S}_k = \sum_{i=0}^{2n} W_i^{(c)} (\hat{\zeta}_k^{(i)} - \mu_k)(\hat{\zeta}_k^{(i)} - \mu_k)^{\mathrm{T}} + \boldsymbol{Q}_k \tag{26}$$

$$\boldsymbol{P}_k^{+} = \boldsymbol{P}_k^{-} - \boldsymbol{K}_k \boldsymbol{S}_K \boldsymbol{K}_k^{\mathrm{T}}. \tag{27}$$

However, in the situation where the measured delay is classified as an outlier, observed values should be treated differently in a manner that reduces the residual most. In this respect, temporal communication delay outliers should be treated carefully since they may influence the plural command signal during the trend. In order to reduce the cumulative uncertainty of the estimation covariance, a rejection strategy was implemented to the update sequence

$$\mathbf{x}_k^{+} = \mathbf{x}_k^{-} = \sum_{i=0}^{2n} W_i^{(m)} \hat{\chi}_k^{(i)} \ \ (\text{if}, \gamma(\theta_o) > \gamma(\theta_p), \tau \geq 2) \tag{28}$$

$$\mathbf{P}_k^{+} = \mathbf{P}_{k-1}^{+}, \tag{29}$$

where $\gamma(\theta_o)$ and $\gamma(\theta_p)$ represent the responsibility of the communication delay outlier and that of the passive delay of the measured delay. It should be noted that in order to activate the rejection strategy before the communication delay is judged as the outlier, the responsibility γ should be confirmed asynchronously for every preliminary determined time.

III. EXPERIMENTAL DESIGN

This section describes a method for evaluating the performance of the proposed filter for communication delay. First, the experimental configuration for measuring the communication delay between the vehicle and the control

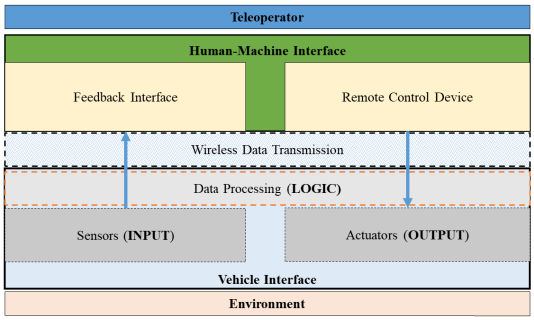

FIGURE 6. Schematic diagram of teleoperation system including a human-machine interface, and a vehicle interface. A stable control strategy is needed considering the communication delay of wireless data transmission.

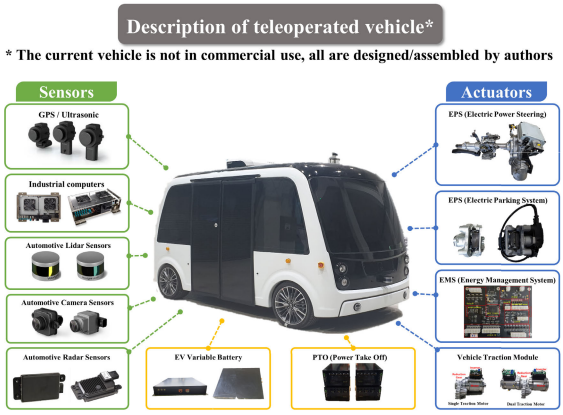

FIGURE 7. Description of the teleoperated vehicle used in the experiment.

center based on GPS is described. Next, to evaluate the performance of the proposed filter, a simulation based on the remote control command transmission experiment and actual communication delay was performed. In the experiment, the control command was transmitted to the remote vehicle to generate the communication delay profiles. Additionally, in the communication delay simulation, the communication delay obtained in the experiment was modeled, and the performance of the proposed filter was evaluated based on the artificially generated communication delay.

A. GENERAL SETUP

Fig. 6, 7 shows teleopration system including the human-machine interface and vehicle interface. First, the remote control device reproduces information from sensors such as wheel angle or speed of the vehicle via a feedback interface. Next, a teleoperator controls the vehicle for the desired mission using the remote control device. Here, the vehicle interface process the command signal received from the remote control device and transfer it to the actuator via controller area network (CAN) format.

Fig. 8 shows used teleoperation system including human-machine interface and vehicle interface. In this study, we adopt a wireless vehicle communication strategy

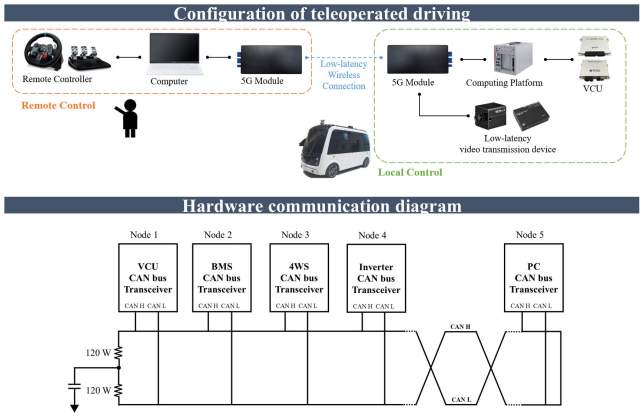

FIGURE 8. Communication and hardware configuration design for the teleoperation. A 5G network band was used to transfer the camera and remote control signal to the teleoperator and vehicle interface.

using a 5G network for camera and remote control signal communication (UX-50C, LG, Korea). As for the local communication, CAN protocol is used to communicate between the vehicle control units (IXXAT compact V2, HMS Networks AB, Sweden). As for the medium operational system for the vehicle interface, ROS-Melodic running on Linux Ubuntu 18.04 LTS (64-bit) was chosen to distribute command signal to each controller units [33]. In addition, a wheel joystick (G29, Logitech, Swiss) was used to feedback and to generate the command signal to the vehicle interface. Also, GPS and used to synchronize clock with local and remote control system (PA1616S, Adafruit, America) with external GNSS antenna (GPS ACTIVE 28dB, Changhong, China). Finally, Chrony[1] and Gpsmon[2] were used to constantly synchronize the internal clock with received clock messages.

B. EXPERIMENT: COMMUNICATION DELAY GATHERING

An experiment was carried out to generate profiles of communication delays based on an actual teleportation system of the vehicle. Fig. 9 shows the experimental setup for generating the communication delay profiles. First, the local control center and the remote vehicle are connected to a 5G/LTE network (Provider, LG, Korea rep.) based on the ROS system. secondly, the control center sends command signal of $\sin(1/25t)$ with synchronized timestamps of 50 Hz interval continuously during 30 minutes. Finally, the remote vehicle receives the control command and computes the communication delay to generate the profiles.

C. SIMULATION: PERFORMANCE TEST UNDER OUTLIER COEXISTENCE USING GAUSSIAN DELAY MODEL

For the performance test of the proposed filter, the stochastic Gaussian mixture model is utilized to generate two or more complicated noise signals. Initially, heavy-tailed Gaussian

[1] https://chrony.tuxfamily.org/
[2] https://gpsd.gitlab.io/gpsd/gpsmon.html

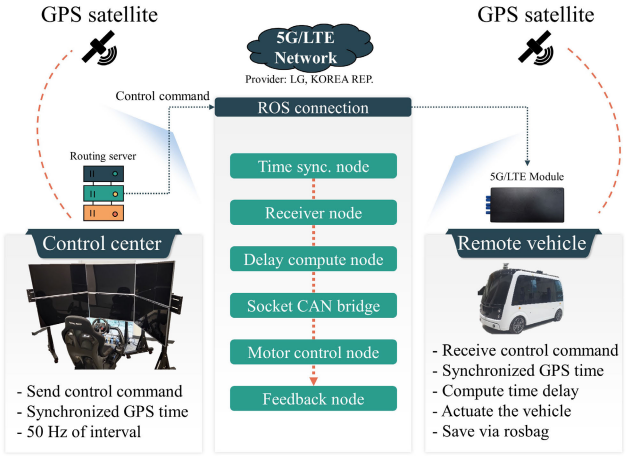

FIGURE 9. Experiment setup for generation of communication delay profiles. Wireless communication condition was managed based on 5G/LTE router with ROS environment.

noise distribution for the communication delay can be modeled with following expression [34]:

$$\boldsymbol{T}_k \sim (1-\psi)\mathcal{N}(\mu_\mathrm{p}, 6_\mathrm{p}) + \psi\mathcal{N}(\mu_\mathrm{o}, 6_\mathrm{o}), \tag{30}$$

where, $\boldsymbol{T}_k$ denotes communication delay at discrete time k, μ_p and μ_o is mean of passive and outlier noise distributions. Also, 6_p, and 6_o are covariance matrices of passive and outlier distributions. ψ represents a contamination ratio of communication delay outlier. However, stochastic modification is needed because the heavy-tailed Gaussian noise distribution is insufficient to mimic the temporary communication outliers.

Secondly, assuming the temporary outlier is affected by a latent variable, stochastic heavy-tailed Gaussian noise is generated as follows:

$$\begin{aligned}\boldsymbol{T}_k \sim\ & (1-\psi)(1-\omega_k)\mathcal{N}(\mu_\mathrm{p}, 6_\mathrm{p}) \\ & + \psi(1-\omega_k)\mathcal{N}(\mu_\mathrm{o}, 6_\mathrm{o}) \\ & + \omega_k\mathcal{N}(\mu_\mathrm{o}, 6_\mathrm{o}),\end{aligned} \tag{31}$$

where, ω_k is a one hot Bernoulli variable depending on latent contamination ratio ρ:

$$p(\omega_k|\rho) = \rho^{\omega_k}(1-\rho)^{1-\omega_k}. \tag{32}$$

Finally, the root means square error (RMSE) computation is used for the evaluation metric for the performance of resisting the outlier:

$$\mathrm{RMSE} = \frac{1}{L}\sum_{k=1}^{L}\sqrt{\frac{1}{N}\sum_{i=1}^{N}(\mathbf{x}_k^i - \hat{\mathbf{x}}_k^i)^2}, \tag{33}$$

where L denotes numbers for the Monte-Carlo simulation trials and N represents the number of simulation samples consisting in each trial. $\mathbf{x}_k^i$ represents the true samples and $\hat{\mathbf{x}}_k^i$ depicts the target samples such as samples that are generated by the stochastic heavy-trailed Gaussian noise or the filter processed samples.

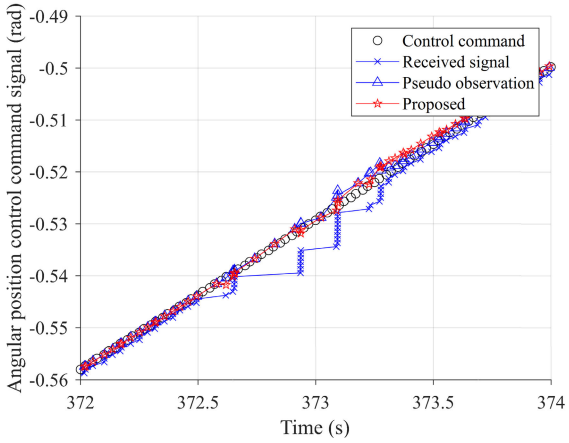

FIGURE 10. Experiment result when applying proposed asynchronous delay compensation Kalman filter.

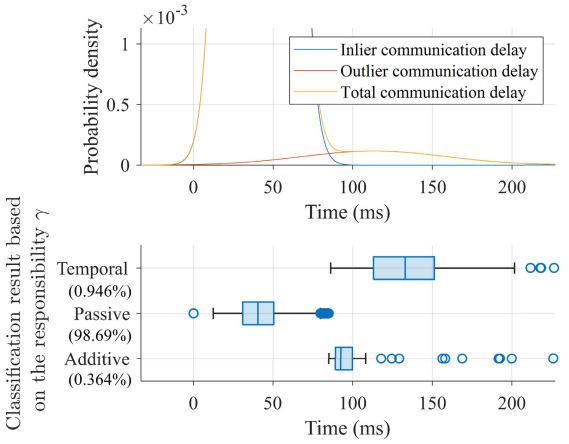

FIGURE 11. Communication delay profile generated by Gaussian mixture model. Responsibility γ is calculated to distinguish the samples into the passive delay, additive delay outlier, and temporary delay outlier.

As for the comparison, the proposed filter is tested Udacity driving dataset of wheel angle samples with time stamps[3] (Sunny, 09/29/2016).

IV. RESULTS

The communication delay measurement was conducted to model the profiles of the delay distributions as shown in Section III. Moreover, each end-to-end ROS master and slave are synchronized to the GPS clock to measure the communication delay. In addition, the constant velocity model was used for the transition function [35], and the initial conditions of Kalman variables were set as follows: error covariance $\mathbf{P}_0 = \mathbf{Q}_k$; initial space state $\mathbf{x}_0$ with $\hat{\mathbf{x}}_0 = \tilde{\mathbf{z}}_0$; measurement noise covariance as $\mathbf{R}_k = \mathrm{diag}(0.05)$; and process noise covariance as $\mathbf{Q}_k = \mathrm{diag}(0.03, 0.03)$; $\alpha = 1$, $\beta = 0$, $\kappa = 0$, $n = 2$.

A. EXPERIMENT: COMMUNICATION DELAY ANALYSIS

Fig. 10, shows a typical scene when the proposed filter encounters a temporary communication delay during the communication delay gathering experiment.

[3]https://github.com/udacity/self-driving-car/tree/master/datasets

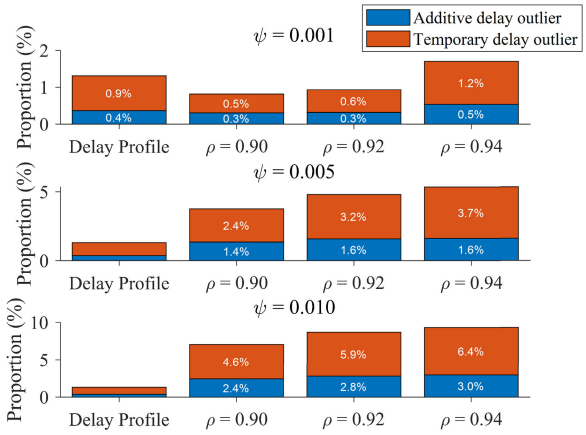

FIGURE 12. A sensitivity analysis was conducted to evaluate the performance of the proposed stochastic heavy-tailed algorithm.

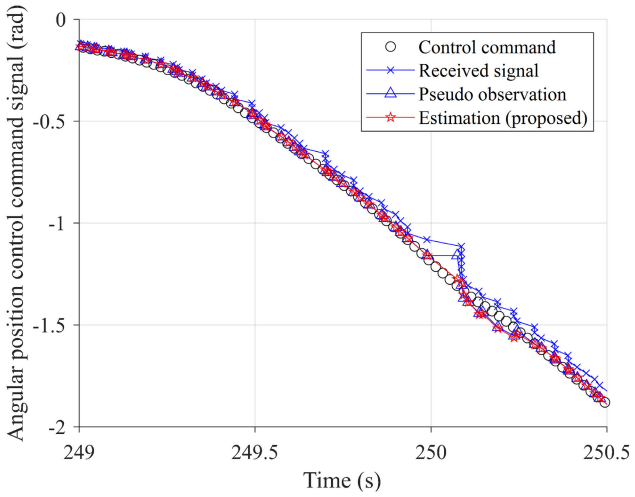

FIGURE 13. Simulation result using the udacity dataset with generated communication delay by stochastic heavy-tailed Gaussian mixture model(ψ : 0.001, ρ : 0.94).

Fig. 11, shows the proportions of passive delay is 98.69% and the communication delay outliers are 1.31% (additive : 0.364%, temporary : 0.946%) among the experiment samples.

Fig. 12 shows additive, and temporary delay outlier proportions against different latent contamination ratios ρ, and contamination ratios ψ. It should be noted that all parameters were tested for 10 trials for 900,000 samples each.

B. SIMULATION: PERFORMANCE TEST USING UDACITY DATASET

Fig. 13 shows a simulation result when applying the proposed filter to the udacity dataset. It should be noted that the communication delay was generated to mimic the delay profile of the measured communication delays (ψ : 0.001, ρ : 0.94).

Fig. 14 shows an error comparison between the udacity dataset with communication delay applied, and the result of

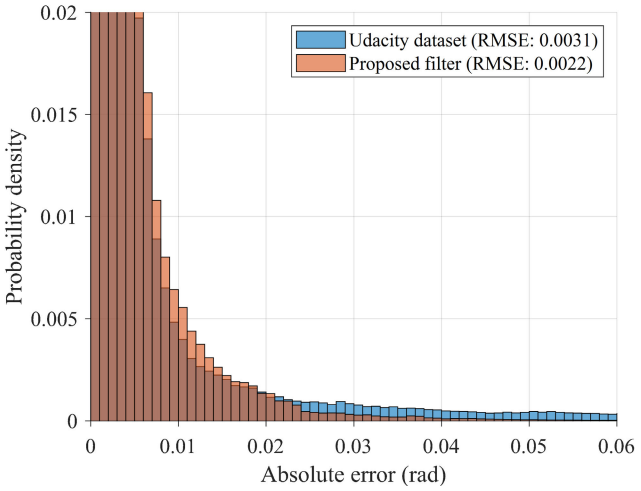

FIGURE 14. Error analysis comparing the udacity dataset with communication delay applied (ψ : 0.001, ρ : 0.94), and the result of the proposed filter.

the proposed filter. The result shows that the RMSE of the proposed filter decreased from 0.0031 rad to 0.0022 rad due to the decrease in probability density for the higher error values.

C. SIMULATION: MONTE-CALRO SIMULATION ANALYSIS

Fig. 15 shows monte-carlo simulation analysis for each latent contamination ratio ρ, and contamination ratio ψ. Note that the simulation was conducted for 100 rounds with 37976 udacity dataset samples with communication delay applied by the stochastic Gaussian delay model.

V. DISCUSSIONS

A. COMMUNICATION DELAY PROFILE AND STOCHASTIC GAUSSIAN DELAY MODEL

As a result of applying the Gaussian mixture model to the measured samples of the communication delays, the borderline for determining the passive and outlier communication delays was found to be 85 ms (see Fig. 11). The result of the communication delay profile shows that although the passive communication delay is dominant (98.69%), the proportions of temporary delays (0.946%) were 2.6 times higher than the additive delays (0.364%) (see Fig. 11). Therefore, it should be emphasized that temporary communication delays deserve more attention not only because of their severity but also from the viewpoint of their chance of emergence. Especially, it is important to remind that the performance of wireless communication can be degraded due to the distance between the receiving stations [36], interferences [37], or the existence of obstacles [38]. Hence, evaluating the performance of wireless systems in extreme conditions is essential such as in scenarios that control the vehicle remotely to reduce the risk until it is acceptable.

In this respect, the proposed stochastic Gaussian delay model can be utilized for reproducing harsh conditions

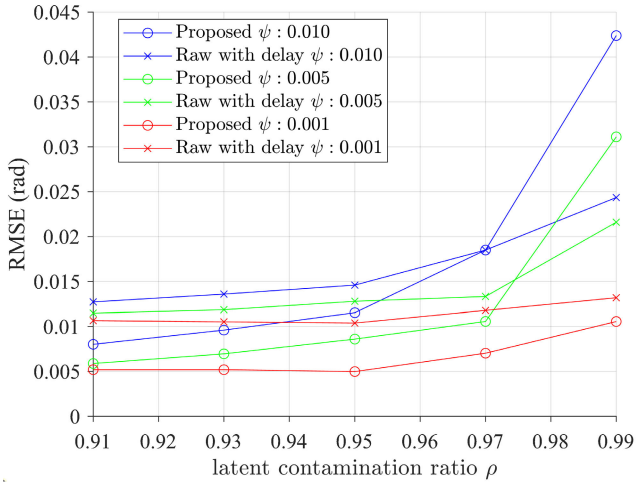

FIGURE 15. Monte-carlo simulation analysis differing latent contamination ratio ρ, and contamination ratio ψ. Each root mean square value was computed for 100 rounds with 37976 udacity dataset samples (L : 100, N : 37976).

because it can control the ratio of temporary communication outliers (31). For instance, when the contamination ratio ψ was 0.010, by increasing the latent contamination ratio ρ from 0.90 to 0.94, the ratio between the temporary and additive communication delays increased from 1.92 to 2.13 (see Fig. 12). However, a precise tune is required for generating a specific ratio of outliers by maintaining the total proportions of outliers because the latent contamination ratio ρ is also responsible for generating the outlier itself. Since increasing the latent contamination ratio ρ increases the total proportions of outliers, reducing the contamination ratio ψ can be effective to maintain the total proportions of outliers. In this respect, it can be said that the proposed stochastic Gaussian delay model has strength in controlling the ratio between the temporary and additive outlier compared to the conventional heavy-tailed Gaussian noise model.

B. PERFORMANCE OF PROPOSED ASYNCHRONOUS DELAY COMPENSATION KALMAN FILTER

As expected, the proposed filter was able to detect the temporary outliers and reject erroneous samples (see Fig. 10, Fig. 13). One of the core properties of temporary outliers is an unexpectable time period of samples to be received. In this regard, an asynchronous feature is essential when judging whether the state can be classified as a hazardous state or not. In accordance with derived communication delay profiles, the proposed filter asynchronously detects the hazardous state and generates the estimated samples based on the transition function of the algorithm (22). As a result of applying the proposed filter, the RMSE decreased by 35% compared to that of the udacity dataset to which the communication delay was added (see Fig. 14). In addition, it can be observed that the highly deviated samples from true values shifted to the smaller absolute error histogram bins and led to an RMSE decrease. Finally, the results of intensive simulation show that the proposed filter is useful even in extreme cases (see Fig. 15). For instance, when the contamination ratio ψ is 0.001, RMSE value of the proposed filter was lower regardless of the value of latent contamination ratio ρ.

C. APPLICATIONS AND LIMITATIONS OF APPROACH

In this study, only the steering wheel-controlling scenario was examined as a target-controlling physical variable. Considering that other core physical parameters such as acceleration or brake pedal control are also a form of signal that follows the communication delay profile, the proposed filter can aid in resisting communication outliers. In addition, not only controlling vehicles from the control center but also the proposed filter is expected to be applied even when conveying road conditions or acceleration information to the control center for realistic vehicle control.

Further, careful consideration should be made before adopting the proposed approach. As shown in the result, in some extreme conditions, the proposed filter may fail to compensate for communication delays (see Fig. 15, when ψ : 0.010, ρ : 0.99). However, considering the ratio of communication outliers are rather high in those conditions (see Fig. 12, when ψ : 0.010, ρ : 0.94 is around 10% of outlier ratio), referencing τ as a judging criterion for an emergency state would be a potential approach to make the system more reliable. For instance, if τ is high enough not to stop the vehicle until it result in a collision, the vehicle should execute the emergency stop to meet the safety requirements.

One another consideration that should be given regarding the dataset used in this study is it only includes 12 minutes of driving data. Possible remote driving conditions in urban scenarios may require rapid and immediate control of the vehicle or relatively long-term controlling of the vehicles. Therefore, intensive validation for different driving behaviors or reliability analysis should be done in the future framework.

D. RELATIONS AND CONSIDERATIONS WITH CURRENT SAFETY STANDARDS

Although ISO 26262 (“Road vehicles – Functional safety”) covers communication delays regarding local communication between vehicle control units, it does not explicitly include delays when controlling the vehicle wirelessly [39]. Therefore, referencing more comprehensive safety standards such as IEC 61508 (“Functional Safety of Electrical/Electronic/Programmable Electronic Safety-related Systems (E/E/PE, or E/E/PES)”) may be a solution to quantitatively validate the performance of the remote controlling system [40]. For instance, IEC 61508 gives guidelines about the average frequency of a dangerous failure of the safety function (For example, SIL2 for $\leq 10^{-7}$ to $\geq 10^{-6}$) while ISO 26262 only gives random hardware failure target values. The proposed method can aid in diminishing the effect of communication delay outliers, but still may not be sufficient to meet the required safety-integrity level. Therefore, to satisfy the desired safety-integrity level of the

remote-controlling system, the overall performance should be improved such as by multiplexing the communication hardware.

VI. CONCLUSION

In this study, we proposed an asynchronous delay compensation Kalman filter that can resist not only additive communication outliers but also temporary communication outliers. In addition, we proposed a stochastic heavy-tailed Gaussian delay model that can control the ratio of additive and temporary outliers. As an experiment, a delay profile gathering experiment and intensive Monte-Carlo simulation were carried out. The result shows that the proposed filter can resist even in extreme conditions where communication delay outliers coexist. The limitation exists where communication delays must be measured precisely and was only tested with the steering controlling scenario. Therefore, our future work includes comprehensive analysis when applied to various control signals adopted in actual teleoperated devices.

ACKNOWLEDGMENT

(Eugene Kim and HyunRok Cha contributed equally to this work.)

REFERENCES

[1] Huawei. (2020). *Smart, Self-driving Cars*. Accessed: Aug. 17, 2022. [Online]. Available: https://www.huawei.com/en/media-center/our-value/smart-cars-the-third-space

[2] Baidu. (2017). *Apollo Open Platform*. Accessed: Aug. 17, 2022. [Online]. Available: https://developer.apollo.auto/

[3] Toyota. (2019). *E-Palette*. Accessed: Aug. 17, 2022. [Online]. Available: https://global.toyota/en/newsroom/corporate/29933371.html

[4] *Surface Vehicle Recommended Practive, Taxonomy and Definitions for Terms Related To On-Road Motor Vehicle Automated Driving Systems*, document SAE-J3016, 2018.

[5] *Taxonomy and Definitions for Terms Related to Driving Automation Systems for On-Road Motor Vehicles*, Standard ISO/SAE PRF PAS 22736, 2021.

[6] State of California department of motor vehicle. (2020). *Autonomous vehicle disengagement reports 2019-2020*. [Online]. Available: https://www.dmv.ca.gov/portal/vehicle-industry-services/autonomous-vehicles/disengagement-reports/

[7] J.-M. Georg and F. Diermeyer, "An adaptable and immersive real time interface for resolving system limitations of automated vehicles with teleoperation," in *Proc. IEEE Int. Conf. Syst., Man Cybern. (SMC)*, Oct. 2019, pp. 2659–2664.

[8] M. Bout, A. P. Brenden, M. Klingegård, A. Habibovic, and M.-P. Böckle, "A head-mounted display to support teleoperations of shared automated vehicles," in *Proc. 9th Int. Conf. Automot. User Interface Interact. Veh. Appl. Adjunct*, Sep. 2017, pp. 62–66.

[9] J.-M. Georg, J. Feiler, F. Diermeyer, and M. Lienkamp, "Teleoperated driving, a key technology for automated driving? Comparison of actual test drives with a head mounted display and conventional monitors," in *Proc. 21st Int. Conf. Intell. Transp. Syst. (ITSC)*, Nov. 2018, pp. 3403–3408.

[10] P. Appelqvist, J. Knuuttila, and J. Ahtiainen, "Mechatronics design of an unmanned ground vehicle for military applications," in *Mechatronic Systems Applications*. 2010, pp. 237–262.

[11] (2020). *Phantom Auto*. [Online]. Available: https://phantom.auto/

[12] R. Muradore and P. Fiorini, "A review of bilateral teleoperation algorithms," *Acta Polytechnica Hungarica*, vol. 13, no. 1, pp. 191–208, 2016.

[13] Z. Ma, Z. Liu, P. Huang, and Z. Kuang, "Adaptive fractional-order sliding mode control for admittance-based telerobotic system with optimized order and force estimation," *IEEE Trans. Ind. Electron.*, vol. 69, no. 5, pp. 5165–5174, May 2022.

[14] S. F. Atashzar, I. G. Polushin, and R. V. Patel, "Networked teleoperation with non-passive environment: Application to tele-rehabilitation," in *Proc. IEEE/RSJ Int. Conf. Intell. Robots Syst.*, Oct. 2012, pp. 5125–5130.

[15] C. Preusche, T. Ortmaier, and G. Hirzinger, "Teleoperation concepts in minimal invasive surgery," *IFAC Proc. Volumes*, vol. 34, no. 9, pp. 409–413, Jul. 2001.

[16] T. B. Sheridan, "Space teleoperation through time delay: Review and prognosis," *IEEE Trans. Robot. Autom.*, vol. 9, no. 5, pp. 592–606, Jun. 2004.

[17] Y. Yao, L. Rao, X. Liu, and X. Zhou, "Delay analysis and study of IEEE 802.11p based DSRC safety communication in a highway environment," in *Proc. IEEE INFOCOM*, Apr. 2013, pp. 1591–1599.

[18] B. Zheng, C.-W. Lin, H. Liang, S. Shiraishi, W. Li, and Q. Zhu, "Delay-aware design, analysis and verification of intelligent intersection management," in *Proc. IEEE Int. Conf. Smart Comput. (SMARTCOMP)*, May 2017, pp. 1–8.

[19] B. Zheng, C.-W. Lin, S. Shiraishi, and Q. Zhu, "Design and analysis of delay-tolerant intelligent intersection management," *ACM Trans. Cyber-Phys. Syst.*, vol. 4, no. 1, pp. 1–27, Jan. 2020.

[20] A. Saifullah, Y. Xu, C. Lu, and Y. Chen, "End-to-end communication delay analysis in industrial wireless networks," *IEEE Trans. Comput.*, vol. 64, no. 5, pp. 1361–1374, May 2015.

[21] Z. Yan, T. Duckett, and N. Bellotto, "Online learning for 3D LiDAR-based human detection: Experimental analysis of point cloud clustering and classification methods," *Auto. Robots*, vol. 44, no. 2, pp. 147–164, Jan. 2020.

[22] N. Bellotto and H. Hu, "Computationally efficient solutions for tracking people with a mobile robot: An experimental evaluation of Bayesian filters," *Auto. Robots*, vol. 28, no. 4, pp. 425–438, May 2010.

[23] N. Bellotto and H. Hu, "Multisensor-based human detection and tracking for mobile service robots," *IEEE Trans. Syst. Man, Cybern., Part B (Cybernetics)*, vol. 39, no. 1, pp. 167–181, Feb. 2009.

[24] G. Chang, "Robust Kalman filtering based on Mahalanobis distance as outlier judging criterion," *J. Geodesy*, vol. 88, no. 4, pp. 391–401, Apr. 2014.

[25] L. Chang and K. Li, "Unified form for the robust Gaussian information filtering based on M-Estimate," *IEEE Signal Process. Lett.*, vol. 24, no. 4, pp. 412–416, Apr. 2017.

[26] H. Wang, H. Li, W. Zhang, and H. Wang, "Laplace l1 robust Kalman filter based on majorization minimization," in *Proc. 20th Int. Conf. Inf. Fusion (Fusion)*, Jul. 2017, pp. 1–5.

[27] H. Wang, H. Li, J. Fang, and H. Wang, "Robust Gaussian Kalman filter with outlier detection," *IEEE Signal Process. Lett.*, vol. 25, no. 8, pp. 1236–1240, Aug. 2018.

[28] Q. Wan, H. Duan, J. Fang, H. Li, and Z. Xing, "Robust Bayesian compressed sensing with outliers," *Signal Process.*, vol. 140, pp. 104–109, Nov. 2017.

[29] E. Kim, Y. Yamada, and O. Shogo, "Robust asymmetric safety Kalman filter for MIMO radar resisting temporary outliers," *IEEE Sensors J.*, vol. 22, no. 19, pp. 18532–18541, Oct. 2022.

[30] G. Bishop and G. Welch, "An introduction to the Kalman filter," *Proc. SIGGRAPH, Course*, vol. 8, nos. 23175-27599, p. 41, 2001.

[31] S. J. Julier and J. K. Uhlmann, "New extension of the Kalman filter to nonlinear systems," in *Signal Processing, Sensor Fusion, and Target Recognition VI*, vol. 3068. Bellingham, WA, USA: SPIE, 1997, pp. 182–193.

[32] D. Mills, *Network Time Protocol*, document RFC-958, 1985.

[33] D. Jiang and L. Delgrossi, "IEEE 802.11p: Towards an international standard for wireless access in vehicular environments," in *Proc. VTC Spring—IEEE Veh. Technol. Conf.*, May 2008, pp. 2036–2040.

[34] Y. Huang, Y. Zhang, N. Li, and J. Chambers, "Robust student'st based nonlinear filter and smoother," *IEEE Trans. Aerosp. Electron. Syst.*, vol. 52, no. 5, pp. 2586–2596, Sep. 2016.

[35] Y. Kim and H. Bang, "Introduction to Kalman filter and its applications," in *Introduction and Implementations of the Kalman Filter*, vol. 1. London, U.K.: IntechOpen, pp. 1–16, 2018.

[36] Z. Xu, X. Li, X. Zhao, M. H. Zhang, and Z. Wang, "DSRC versus 4G-LTE for connected vehicle applications: A study on field experiments of vehicular communication performance," *J. Adv. Transp.*, vol. 2017, no. 1, pp. 1–10, 2017.

[37] G. Boudreau, J. Panicker, N. Guo, R. Chang, N. Wang, and S. Vrzic, "Interference coordination and cancellation for 4G networks," *IEEE Commun. Mag.*, vol. 47, no. 4, pp. 74–81, Apr. 2009.

[38] F. Righetti, C. Vallati, D. Comola, and G. Anastasi, "Performance measurements of IEEE 802.15.4g wireless networks," in *Proc. IEEE 20th Int. Symp.*, Jun. 2019, pp. 1–6.
[39] *Road Vehicles—Functional Safety*, document ISO 26262, 2018.
[40] *Functional Safety of Electrical-Electronic/Programmable Electronic Safety-Related Systems*, document IEC 61508, 2010.

EUGENE KIM received the Ph.D. degree in system mechanical engineering from Nagoya University, Nagoya, Japan, in 2021. He is currently with the Automotive Materials & Components Research and Development Group, Korea Institute of Industrial Technology. His research interests include functional/inherent safety of machinery, safety-related sensor systems, and automotive/remote driving vehicles.

HYUNROK CHA received the Ph.D. degree in physics from Tokyo Institute of Technology, Tokyo, Japan, in 2009. He is currently the Director of Seonam Division, Korea Institute of Industrial Technology. His research interests include E-mobility, electric vehicle platforms, smart vehicle control hybrid-powered drones, and power electronics.

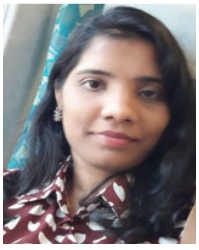

TERESSA TALLURI received the master's degree in thermal engineering from Jawaharlal University, India, and the Ph.D. degree from Busan University, South Korea, in 2022. She is currently pursuing the Ph.D. degree with UST, Korea Institute of Intudstiral Technology. She was an Assistant Professor with KL University, India. Her research interests include hybrid autonomous electric vehicles and electric vehicles.

CHANYEONG JEONG received the B.S. and M.S. degrees in mechanical engineering from Gwangju Institute of Science and Technology (GIST), Gwangju, South Korea, in 2018 and 2020, respectively. He is currently with the Automotive Materials & Components Research and Development Group, Korea Institute of Industrial Technology.

HYEONWOO KIM received the B.S. and Ph.D. degrees in mechanical engineering from Sungkyunkwan University, South Korea, in 2013 and 2016, respectively. He is currently with the Automotive Materials & Components Research and Development Group, Korea Institute of Industrial Technology.

SEUNGHA YOON received the Ph.D. degree from Gwangju Institute of Science and Technology (GIST), Gwangju, South Korea, in 2014. He involved with LG Electronics, Sensor Solution Laboratory, South Korea, until 2019. He is currently a Senior Researcher with Korea Institute of Industrial Technology.

MYEONGHWAN HWANG received the Ph.D. degree in electrical engineering from Chonnam National University, South Korea, in 2021. He is currently with the Automotive Materials & Components Research and Development Group, Korea Institute of Industrial Technology. His research interests include hybrid electric vehicles (HEVs) electric vehicles (EVs) and motor drive systems.